Transient Recovery Voltages in Vacuum Circuit Breakers Generated by the Interruption of Inrush Currents of Large Motors

A. Borghetti, F. Napolitano, C.A. Nucci, M. Paolone, M. Sultan, N. Tripaldi

***Abstract*—The switching of medium voltage electrical motors is typically realized by means of vacuum circuit breakers (VCBs) essentially in view of their elevated number of switching cycles. As known, switching of VCBs generates important transient recovery voltages (TRVs) that need to be properly evaluated for both VCB sizing and insulation coordination. As large medium voltage electrical motors are installed into plants typically controlled by means of Supervisory Control And Data Acquisition (SCADA) systems, maneuvers that involve the motor inrush followed by its sudden de-energization (due to the intervention of an automatic diagnostic function), results into important TRVs. The paper aims at investigating the TRVs due to this specific type of VCB switching by means of a model that has been developed for the purpose, and has then been implemented in the EMTP-RV simulation environment. The validation of the implemented models makes reference to a real plant, and is obtained by comparing the simulation results with some experimental transients provided by the plant data fault recorder. The paper finally discusses the adequacy of different countermeasures by analyzing their effectiveness for the TRVs limitation.**

***Keywords*: vacuum circuit breakers, transient recovery voltages, motor inrush currents, EMTP simulations.**

I. Introduction

TRANSIENT recovery voltages (TRVs) in vacuum circuit breakers (VCBs) appear to be still a concern for the operation of some power plants with peculiar characteristics. Several international standards have been recently updated for the correct breaker sizing (e.g. [1-3]). The procedures described in the above-mentioned standards cover the majority of the breaker operating conditions. However, peculiar system configurations combined with specific VCB dielectric strength recovery and ability to chop high-frequency arc currents, could generate cases in which TRVs could exceed the VCB withstand capability and re-ignition phenomena could take place.

On the specific topic of motor switching operated by VCBs, several studies have been already presented in the literature: in [4] the switching performances of MV circuit-breakers (SF_6 and VCB technology) are examined by using the Cigré WG 13.02 motor model; in [5] the effectiveness of various protection countermeasures against TRVs in VCB switched motors are evaluated together with a sensitivity analysis with reference to different electrical network and motor parameters; in [6,7] the TRVs due to the early-interruption of the inrush currents of a large motor fed by a transformer are studied.

This paper deals with this last type of switching maneuvers that may take place when the operation of large plants is automatically controlled by a Supervisory Control And Data Acquisition (SCADA) system. If the operator requests to energize a specific motor in presence of a generic diagnostic failure, the motor energization is followed by its sudden de-energization automatically operated by the SCADA and the two maneuvers are typically separated by a time interval in the order of few tens of ms. In such a condition, the motor breaker is requested to interrupt a large inductive current also characterized by the presence of a superposed a-periodic component. In case the motor is supplied through a transformer, the non-linear transformer inrush current is also present.

In order to carry out the analysis of these type of TRVs, a detailed model of the section of a large water pumping plant has been implemented in the EMTP-RV simulation environment [8,9] together with a detailed VCB model.

The structure of the paper is the following: section II illustrates the problem of interest; section III describes the implemented VCB model, section IV illustrates the model of the plant — including all the main components, namely: the high voltage and medium voltage cable lines, the substation transformers, the transformers, the water pumps motors etc. — and its validation by means of the comparisons of the simulation results with some TRVs transients provided by the plant data fault recorder; section V discusses the effectiveness of various countermeasures to limit the TRVs and section VI concludes the paper.

II. The problem of interest

As mentioned in the Introduction, the paper aims at analyzing the TRVs that could take place in case a VCB is

A. Borghetti, F. Napolitano, C.A. Nucci and M. Paolone are with the Department of Electrical Engineering, University of Bologna, Bologna, Italy (e-mail: {alberto.borghetti; fabio.napolitano; carloalberto.nucci; mario.paolone}@unibo.it).

M. Sultan is with the Saudi Aramco, Saudi Arabia, (e-mail: mansour.sultan@aramco.com).

N. Tripaldi is with Saipem S.p.A., Fano, Italy (e-mail: nazareno.tripaldi@saipem.eni.it).

Paper submitted to the International Conference on Power Systems Transients (IPST2011) in Delft, the Netherlands June 14-17, 2011

operated to interrupt the inrush current of a motor fed through a power transformer.

The problem can be sketched by means of the simplified network configuration illustrated in Fig. 1a. The MV feeding network supplies a large induction or synchronous motor by means of a step-down transformer. The energization and de-energization of the motor is operated by means of a VCB that interconnects the feeding network and a suitable cable line. The equivalent circuit of such a network is shown in Fig. 1b in which the inrush operation of the motor has been represented, in a first approximation, by its locked-rotor impedance. The meaning of the parameters is the following: R_{sc} and X_{sc} are the real and imaginary parts of the network short circuit impedance, R_{cbl}, X_{cbl} and C_{cbl} are the parameters (in general frequency-dependent) of the cable line, R_{sct} and X_{sct} are the real and imaginary parts of the transformer short circuit impedance, R_{mag} and X_{mag} are the real and imaginary parts of the transformer magnetization impedance (X_{mag} is non-linear), R_{lrm} and X_{lrm} are the real and imaginary parts of the locked-rotor motor impedance.

It is worth noting that the equivalent circuit shown in Fig. 1b aims basically at illustrating qualitatively the phenomenon of interest. Indeed, it does not include the complex transformer model usually required in order to accurately reproduce the behavior of such a component in presence of high-frequency electromagnetic transients (e.g. [10-15]) as well as the high-frequency response models of the other network components.

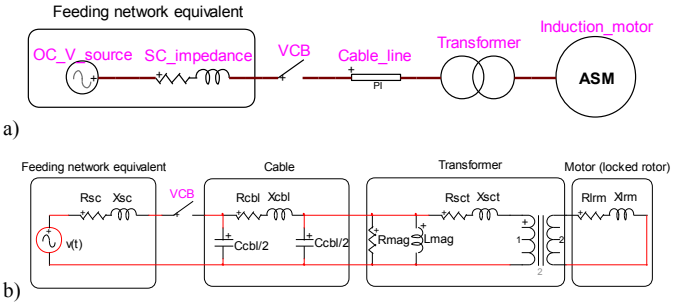

Fig. 1. a) Network configuration for the problem of interest; b) simplified equivalent circuit.

The circuit shown in Fig. 1b produces an inrush current through the VCB that is the result of the inrush current of the motor itself superposed to the inrush current of the transformer. Therefore, the resulting current is characterized by the presence of:

- two a-periodic components: the first due the energization of the locked rotor impedance R_{lrm} and X_{lrm} and the second due to the energization of the non-linear inductance X_{mag};
- two periodic steady state components: the first given by the locked rotor impedance (essentially sinusoidal with a single spectrum component), the second (highly distorted), due to the non-linearity transformer core inductance X_{mag};
- as a function of the amplitude ratio between the a-periodic and periodic components and of the time interval between the VCB close-open maneuvers, the zero-crossings of the current waveform are shifted from their symmetrical position and, therefore, the chopping of the inrush current could take place in correspondence of a non-symmetrical position.

These characteristics are different from those of the current waveforms produced in out-of-phase switching tests and cannot be easily treated by means of analytical approaches. However, they could be reproduced and analyzed by using specific EMTP models.

III. VCB MODEL AND ITS IMPLEMENTATION

A. VCB model summary

As suggested in the literature and international standards on the subject (e.g. [16-18]), three main characteristics of VCBs have been taken into account in the implemented model:

1. the chopping current value;
2. the cold withstand voltage characteristic (or cold gap breakdown voltage);
3. the high frequency current quenching capability.

Concerning the first point, the value of the chopping current depends on different parameters, such as the contact material or the load surge impedance (e.g. [19]). In the implemented model, a constant value of the chopping current has been assumed, although it may be considered as statistically distributed. In [19], for example, an expression of the mean value of the chopping level has been proposed.

The second important aspect in the VCB modeling is the representation of the dielectric strength associated with the open contacts in the vacuum. In [21,22] it has been concluded that, when the preceding arc current does not exceed several hundred Amperes, the consequent breakdown voltage under the influence of the TRV, the frequency of which is within few kHz, is equivalent to the cold withstand voltage characteristic. This characteristic depends on the distance between the contacts and, therefore, it change with time according to the contacts separation speed [22,23]. The statistical distribution of this characteristic is analyzed in [24].

Different expressions have been adopted in the literature to represent the cold withstand voltage characteristic as a function of time:

- linear expression (e.g. [19,21]);
- exponential expression (e.g. [24]).

As the re-ignition takes place at short gaps (< 1 mm), the difference between the two expressions could be considered negligible. Therefore, the linear expression may be considered enough accurate to represent this VCB characteristic (e.g. [17]). Such a representation is also adopted by IEEE Standards [1] and [2] and the values of its parameters are typically provided by VCB manufacturers or, in case of available experimental data, by means of suitable fitting between measured and model-simulated transients.

The implemented linear expression of the VCB cold-

withstand voltage characteristic is:

$$U = A\left(t - t_{open}\right) + B \tag{1}$$

where:

- t_{open} is the time from contact separation;
- A is the rate of rise of dielectric strength;
- B is the TRV withstand just before the contact separation.

Concerning the third point, the VCB high-frequency quenching capability is defined by the slope of the high frequency reignited current at current zero. This parameter is needed as re-ignitions occur when the TRVs exceed the dielectric strength of the breaker contacts. This leads to high frequency current components superimposed to the power frequency current. The high frequency quenching capability of typical VCBs is found to be in the range of several hundred A/μs. The quenching capability of VCB is represented by using the following known equation [21]:

$$\left(\frac{di}{dt}\right)_{HF} = C\left(t - t_{open}\right) + D \tag{2}$$

where:

- C is the rate of rise of VCB high frequency quenching capability;
- D is the VCB quenching capability just before its contact separation.

The values of parameters *A, B*, *C* and *D* depend on the specific VCB [17].

The model includes also a RLC branch in parallel to the VCB in order to take into account the open contact gap stray capacitance, resistance and relevant inductance. The values of the parameters of this RLC branch usually adopted in the literature are: R_s=100 Ω, L_s=50 nH and C_s=100 pF.

B. VCB model implementation

The implementation of the VCB model into the EMTP-RV environment is shown in Fig. 2. It adopts a controlled switch for each VCB phase/pole ('VCB_ph_a' in Fig. 2). In order to reproduce the VCB characteristics described in the previous subsection, the status of each controlled switch is determined by a flip-flop logic block that changes the VCB closed or open statuses depending on the output of two blocks: 'VCB_ph_a_closing' and 'VCB_ph_a_opening', which will be described next. Additionally, a standard switch is inserted in series with the controlled switch ('SW1' in Fig. 2) to simulate the closing command to the VCB. To disconnect the RLC branch in parallel to the VCB a controlled switch ('cSW4' in Fig. 2) is connected in series with this branch and its status is determined by inverting the logic control of the VCB phase/pole.

Block 'VCB_ph_a_closing' represents the VCB re-ignition by setting the closing command to the flip-flop and, therefore, to 'VCB_ph_a', according to the condition

$$\left|v_{ph\_a}(t)\right| > U_{ph\_a}(t) \tag{3}$$

where:

- $v_{ph\_a}(t)$ is the instantaneous value of the voltage across the VCB phase/pole *a*;
- $U_{ph\_a}(t)$ is the instantaneous value of the cold withstand voltage characteristic of VCB phase given by (1).

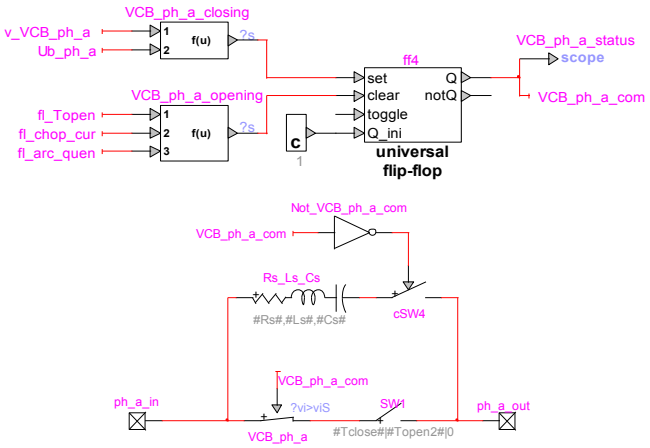

Fig. 2. EMTP-RV implementation of the VCB model.

It is worth noting that value of $U_{ph\_a}(t)$ provided by (1) is calculated for $t > t_{open}$ and it is bounded by the maximum TRV capability value provided by the VCB manufacturer (variable '*Ub_limit*').

Block 'VCB_ph_a_opening' sets the open command to the flip-flop, and therefore to VCB_ph_a, if the three input logic variables 'fl_Topen', 'fl_chop_cur' and 'fl_arc_quen' are true at the same time.

'fl_Topen' is true only when $t > t_{open}$.

'fl_chop_cur' is true only if:

$$\left|i_{ph\_a}(t)\right| < i_{ph\_a}^{chop} \tag{4}$$

where:

- $i_{ph\_a}(t)$ is the instantaneous value of the current passing through the VCB phase/pole *a*;
- $i_{ph\_a}^{chop}$ is the chopping current of the VCB phase/pole *a*.

'fl_arc_quen' is true if

$$\left|\frac{di_{ph\_a}(t)}{dt}\right|_{i_{ph\_a}(t)=0} < \frac{di_{ph\_a}^{quench}(t)}{dt} \tag{5}$$

where:

- $di_{ph\_a}(t)/dt\big|_{i_{ph\_a}(t)=0}$ is the value of the zero-crossing time derivative of the current passing through the VCB phase/pole *a*;
- $di_{ph\_a}^{quench}(t)/dt$ is the instantaneous value of the high frequency current quenching capability of the VCB phase/pole provided by equation (2).

Fig. 3 shows the EMTP-RV scheme that implements this control function.

As done for the cold withstand voltage characteristic, also the value of the high frequency current quenching capability of the VCB has been upper-bounded (variable '*arc_qu_limit*'). As this parameter is generally unknown, it has been tuned

according to the available measurements as described in the next section.

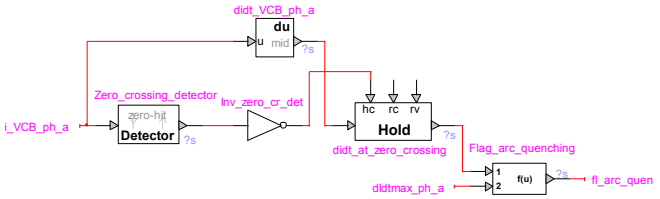

Fig. 3. Control function that checks whether the absolute value of the VCB current time derivative at zero crossing is lower than the VCB high frequency current quenching capability.

IV. Network Model and its Validation for TRV Studies

A. Description of the plant model

The studied network refers to a water pump plant and its simplified scheme is shown in Fig. 4. The network is composed by a main 230/34.5 kV substations (fed by a 230 kV equivalent network) equipped with two 230/34.5 kV transformers (T1 and T2) providing the supply to two busses, B1 and B2, to which four 14.3 MVA synchronous motors (M1 to M4) are connected through 25 MVA 34.5/13.8 kV transformers (TM1 to TM4). The connection between each motor transformer and the relevant VCB (Br_M1 to Br_M4) is realized by three parallel cable lines (coaxial type).

On the same 34.5 kV side of the substation, other loads are supplied through 15 MVA 34.5/4.16 kV transformers (Tlv2 to Tlv5) or 2.5 MVA 34.5/0.48 kV (Tlv1) transformers.

The frequency-dependent (FD) cable model [25] has been adopted to represent the both 230 kV and 34.5 kV coaxial cables, in order to adequately reproduce their high frequency behavior associated to the transients produced by the switching maneuvers. For the evaluation of the cable line modal characteristic impedances $Z_{c,i}$ and propagation constant $A_{p,i}$ we assume:

- the ground resistivity equal to 146 Ω·m;
- a frequency range from 0.01 Hz to 10 MHz;
- a logarithmic frequency range decomposition;
- 10 points per decade in which $Z_{c,i}$ and $A_{p,i}$ are calculated;
- 30 poles adopted for the approximations of $Z_{c,i}$ and $A_{p,i}$.

In order to provide a first verification of the cable models, a comparison with the phase-to-shield surge impedances values provided by the cable manufacturer, determined at 60 Hz, has been performed:

- 230 kV cable manufacturer data Z=64.8 Ω, implemented model Z=62.8 Ω;
- 34.5 kV cable manufacturer data Z=44.3 Ω, implemented model Z=40.67 Ω.

The network transformers have been modeled in order to represent both their 60 Hz steady state behavior and their response to high frequency transients. The steady state behavior has been represented by means of a standard transformer equivalent circuit representing the winding connections as well as the transverse parameters (magnetization current and core losses), the parameters of which have been inferred from the manufacturer data. Concerning transformers TM1 to TM4, the non-linear transformer core reactance has been taken into account and its values has been tuned in order to match the measured inrush currents. The high frequency response of the transformers has been represented, in a first approximation, by introducing into the model a specific Π-circuit of capacitances as suggested in [1].

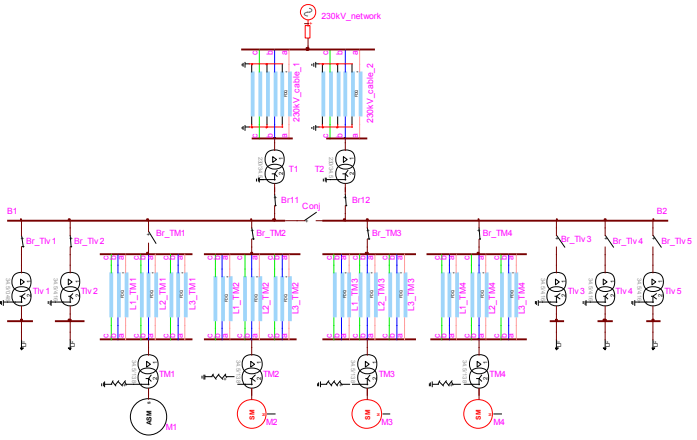

Fig. 4. Scheme of the simulated power network.

The motors have been represented by using two different models available in the EMTP-RV library. As the plant motors are of synchronous type, the machines assumed to be in operation have been represented using the model proposed in [25,26]. The starting motor (for which the inrush current is mainly of interest) is represented by the induction-motor model of [27,28]. The parameters of both machines models have been inferred by using manufacturer data.

B. Network and VCB models validation

The data provided by the plant digital fault recorder (DFR) have been used to tune the values of various parameters of the VCB model that are not typically provided by manufacturers and to validate the complete network model.

Parameters A and B of (1), as well the threshold of the VCB chopping current and cold-withstand voltage (*Ub_limit*), have been inferred from the VCB manufacturer data:

- chopping current=3.5 A;
- $A = 56.8 \cdot 10^7$ V/s;
- $B = 0$;
- *Ub_limit*=71 kV.

Parameters C, D and the threshold of the quenching capability (*arc_qu_limit*) have been tuned to fit the DFR measurements within the range of values mentioned in the literature as typical (e.g. [17]):

- $C = 31 \cdot 10^{10}$ A/s^2;
- $D = 155 \cdot 10^6$ A/s;
- *arc_qu_limit*=$135 \cdot 10^6$ A/s;

Fig. 5 shows the comparison between simulations and measurements relevant to the voltages and currents in

correspondence of breaker Br11 during the energization of the motor M1 of Fig. 4. The reproduced maneuver is the following: initially motors TM2 and TM3 are not in operation whilst motor TM4 is in operation; all the transformers are energized with the exception of Tlv3. Tie-breaker 'Conj' is open. Motor TM1 is energized by closing the VCB Br_TM1 at t=53 ms. The same circuit breaker is suddenly opened at 95 ms. It is worth noting that, in agreement with the DFR measurements, different closing times have been adopted for the three VCB poles[1].

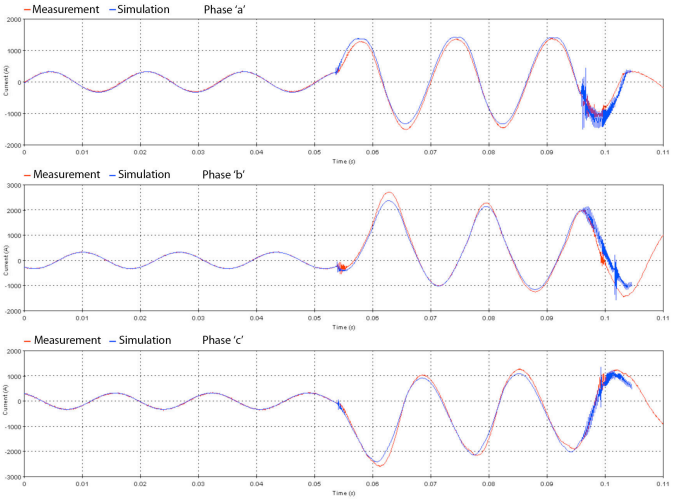

Fig. 5. Comparison between simulated (blue curves) and DFR measured (red curves) currents in correspondence of breaker 'Br11' of Fig. 4 during the energization of the motor M1.

In view of the complexity of the involved non-linear phenomena and uncertainty on the knowledge of the various VCB parameters, the obtained comparison between simulations and measurements can be considered satisfactory. In particular, the obtained results show that the developed model is able to reproduce correctly the asymmetrical opening of VCB Br_TM1 phase/pole *a* and the re-ignitions in phases/poles *b* and *c*. In this respect, it is worth observing that (i) the DFR is down-sampling the transient phenomena that take place during closing and opening maneuvers of the VCBs as it is sampling at 23040 Hz, (ii) the bandwidth characteristics of the transducers, which output signals are collected by the DFR, are unknown. Concerning this last point, it is worth noting that typical voltage/current transformers are characterized by a quite limited bandwidth with upper limits in the order of few kHz and could be characterized by transfer function that exhibit frequency resonances in the kHz range (e.g. [32]).

In order to complete the set of simulation results, Fig. 6a shows a time-zoom of the currents flowing through the VCB as well as the voltages across the VCB poles. In particular, these results show the re-ignitions taking place after the VCB opening.

As it can be seen from Fig. 6b, the voltage rise-time across the VCB poles is in the order of 260 µs. This quite high value is essentially due to the capacitance of the cable between the VCB and the transformer. Such a TRV rise has an average time derivative of $27 \cdot 10^7$ V/s, which is half of the rate of rise of VCB dielectric strength (parameter A of equation (1)). therefore, the increase of the VCB maximum TRV capability (parameter '*Ub_limit*'), in spite of the TRVs rate of rise, can be considered as an effective countermeasures to avoid current re-ignitions,.

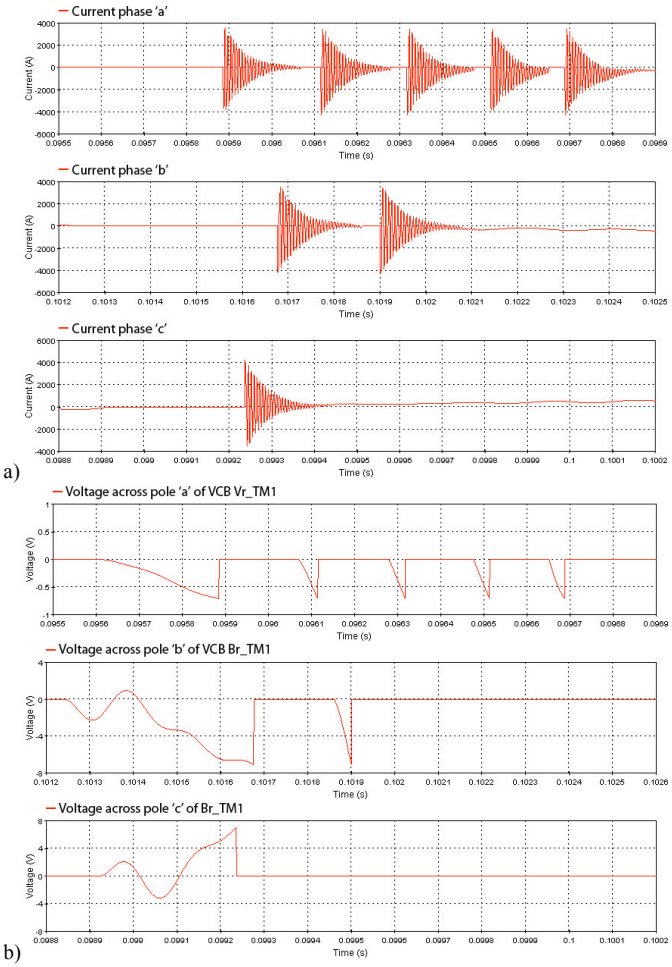

Fig. 6. Time-zoom in correspondence of the VCB currents re-ignitions taking place after the opening maneuver of breaker 'Br11' of Fig. 4 during the energization of the motor M1: a) currents flowing through the VCB, b) voltages across the VCB poles.

V. Analysis of Possible Countermeasures to Limit the TRVs

This section of the paper analyzes the possible countermeasures to avoid the presence of re-ignitions

[1] The energization of the shipping motor (VCB closing maneuver) involves the presence of overvoltages due to the sequential closing of the circuit breaker poles. Several examples of these overvoltages are illustrated and discussed in the literature on the subject (e.g. [29-31]). In particular, the results of these studies show that the origin of the largest overvoltages is due to the closing of the second and third breaker poles in correspondence of the peak value of the overvoltage originated by the closing of the first breaker pole. A similar behavior has been observed in the results obtained with the implemented model.

subsequent to the VCB interruption of the motor inrush currents, namely:

a. increase of the TRV capability of the VCB up to 80 kV;
b. connection of snubber circuits installed at the load side of the VCB.

A. Countermeasure a: increase of the TRV capability

In order to infer the TRV capability up to which the VCB could withstand the TRVs of interest (in spite of the TRVs rate of rise), a statistical study has been performed by varying the VCB closing-opening time. The results have shown that the maximum amplitude of TRV does not exceed 80 kV. We here present the results obtained by using this value to set the VCB parameter '*Ub_limit*' (see section III) into the EMTP model relevant to the simulation of the energization of the motor M1 operated by VCB Br_TM1. Fig. 7a shows the Br_TM1 currents during the whole transient and Fig. 7.b shows the TRVs in correspondence of the current interruption. The VCB performs a successful opening without current re-ignitions.

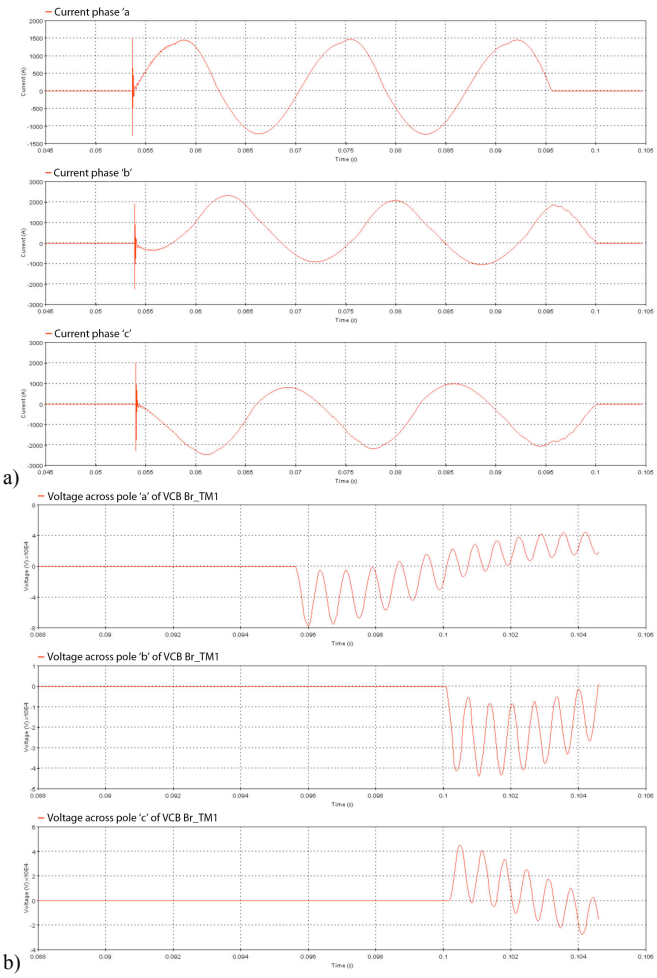

Fig. 7. VCB Br_TM1 currents (a) and voltages (b) during the successful interruption of the energization current of the motor M1 using a VCB TRV capability of 80 kV.

A. Countermeasure b: snubber circuits

The adoption of the so-called snubber circuits, or RC surge suppressor, is one of the solutions typically presented in the literature on the subject to reduce the amplitude of TRVs (e.g. [1,22,33]). This solution is particularly effective as it changes the self-oscillation frequency of the part of the disconnected circuit and, therefore, directly influences both TRV amplitudes and raise-times.

Values typically adopted in the literature for these components ranges between 30-100 Ω for the resistance and 0.3-1 μF for the capacitance.

The following values have been selected and compared in terms of effectiveness for the TRVs reduction:

- R= 50 Ω, C=0.5 μF;
- R= 250 Ω, C=0.5 μF;
- R= 90 Ω, C=1.1 μF;
- R= 130 Ω, C=1 μF.

Fig. 8 shows the simulated TRVs due to the interruption of the inrush current of the motor M1 without the RC snubber and for the four different RC values above selected. In these simulations, the RC snubber has been considered placed on the load side terminals of the VCB Br_TM1. It is worth noting that, due to the relative short cable length that connects the VCB to the captive transformers, the effectiveness of these devices remains unchanged even if they are connected in correspondence of the 34.5 kV terminals of the motor transformer.

Table I reports the maximum TRV values of Fig. 8 together with the three-phase active and reactive power absorption of each RC snubber circuit in steady state conditions. The results of Table I and Fig. 8 allow to infer that the best balance between TRV mitigation and minimum reactive power injection in steady state is achieved by using the parameters R=130 Ω, C=1 μF or R= 250 Ω, C=0.5 μF.

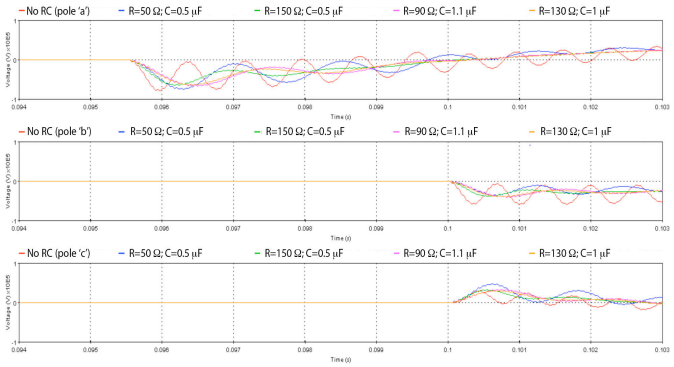

Fig. 8. TRVs across the VCB Br_TM1 contacts during the interruption of the energization current of the motor M1 using different values of RC snubber parameters (snubber circuit installed in correspondence of the load side of the VCB).

We now present the results obtained by using RC values b) and d), namely R=250 Ω, C=0.5 μF and R=130 Ω, C=1 μF, for the analysis of the energization of the motor M1 operated by Br-TM1.

In particular, Fig. 9a shows the VCB TRV in correspondence of the current interruption for the snubber b) (R=250 Ω, C=0.5 μF) and Fig. 9b shows the same quantities

for the snubber d) (R=130 Ω, C=1 μF). As it can be observed, the VCB performs a successful opening without re-ignition phenomena (the maximum value of the TRV is of 63.5 kV for the snubber b) and of 63 kV for the snubber d).

TABLE I: MAXIMUM TRVS VALUES INFERRED FROM FIG. 8 (PHASE A ONLY) TOGETHER WITH THE THREE-PHASE ACTIVE AND REACTIVE POWER ABSORPTION OF EACH RC SNUBBER CIRCUIT. SNUBBER CIRCUIT INSTALLED IN CORRESPONDENCE OF THE LOAD SIDE OF THE VCB.

RC value	Maximum TRV [kV]	Absorbed three phase power in steady state conditions	
		P [kW]	Q [kVar]
without RC	78.6	-	-
R= 50 Ω, *C*=0.5 μF	74.9	2	-224
R= 250 Ω, *C*=0.5 μF	64.9	11	-224
R= 90 Ω, *C*=1.1 μF	66.7	18	-493
R= 130 Ω, *C*=1 μF	64.4	22	-448

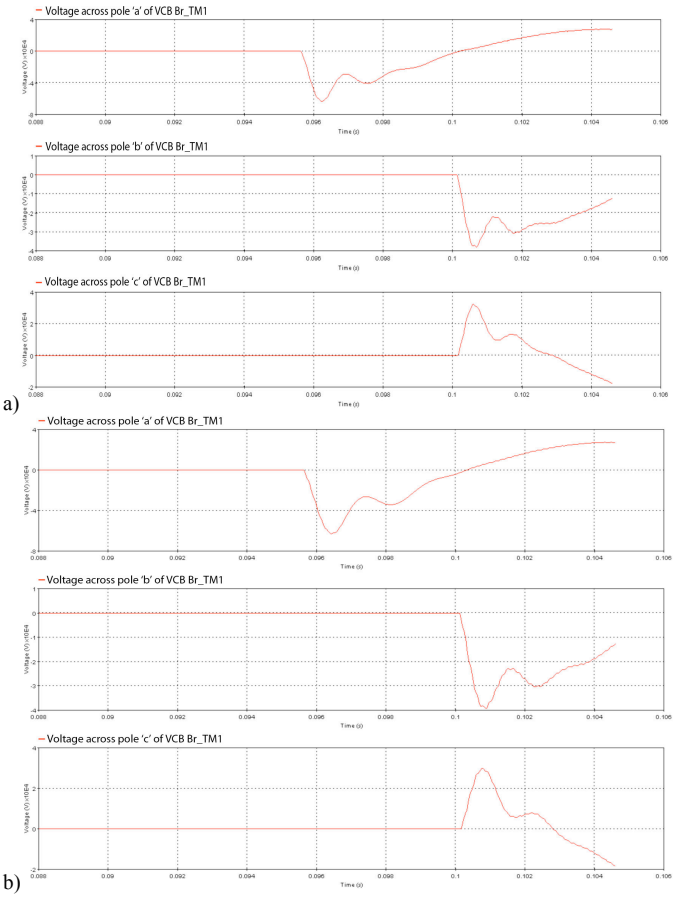

Fig. 9. VCB Br_TM1 voltages during the successful interruption of the energization current of the motor M1 using a VCB TRV capability of 80 kV: (a) snubber b) with *R*=250 Ω, *C*=0.5 μF; (b) snubber d) with *R*=130 Ω, *C*=1 μF).

VI. CONCLUSIONS

The paper has presented the implementation of a VCB model and of the electrical system of a water pumping plant into the EMTP-RV simulation environment aimed at analyzing the TRVs generated by the early interruption the inrush currents of large motors.

The implemented model has been validated by comparing the simulation results with the experimental data provided by a Digital Fault Recorder (DFR) system installed into the plant.

The results of these simulations have shown that TRVs associated to the interruption of motor inrush currents are of concern for the VCB opening maneuver as they can result into VCB re-ignitions. The analyzed countermeasures are:

a. increase of the TRV capability of the VCB up to 80 kV;
b. connection of snubber circuits installed at the load side of the VCB.

Both countermeasures have been proved adequate for the solution of the problem. The paper also suggests the parameters needed to select the components to be adopted in each one of these solutions and highlighted how important is the detailed modeling of the system in addition to that of the circuit breaker.

VII. REFERENCES

[1] IEEE Std. C37.011, IEEE Application Guide for Transient Recovery Voltage for AC High-Voltage Circuit Breakers, 2005.

[2] IEEE Std. C37.06, IEEE Standard for AC High-Voltage Circuit Breakers Rated on a Symmetrical Current Basis – Preferred Ratings and Related Required Capabilities for Voltages above 1000 V, 2009.

[3] IEEE Std. C37.04, IEEE Standard Rating Structure for AC High-Voltage Circuit Breakers, 1999 (R2006).

[4] J.D. Gibbs, D. Koch, P. Malkin, K.J. Cornick, "Comparison of performance of switching technologies on E Cigre motor simulation circuit", IEEE Trans. on Power Delivery, vol. 4-3, July, 1989, pp.1745 – 1750.

[5] D. Penkov, C. Vollet, B. De Metz-Noblat, R. Nikodem, R., "Overvoltage protection study on vacuum breaker switched MV motors", Proc. of the 5th Petroleum and Chemical Industry Conference Europe - Electrical and Instrumentation Applications, PCIC Europe 2008.

[6] M. Venu Gopala Rao, S.A. Naveed, J. Amaranath, S. Kamakshaiah, B.P. Singh, "Reduction of switching transients in the operation of induction motor drives", Proc of the 12th International Symposium on Electrets, 2005, pp: 388 – 391.

[7] R. B. Lastra, M. Barbieri, "Fast Transients in the Operation of an Induction Motor with Vacuum Switches", Prof. of the Int. Conf. on Power Systems Transients IPST 2001, 24-28 June 2001, Rio de Janeiro (Brasil), paper 063.

[8] J. Mahseredjian, S. Lefebvre and X.-D. Do, "A new method for time-domain modelling of nonlinear circuits in large linear networks", Proc. of 11th Power Systems Computation Conference PSCC, August 1993.

[9] J. Mahseredjian, S. Dennetière, L. Dubé, B. Khodabakhchian and L. Gérin-Lajoie: "On a new approach for the simulation of transients in power systems". Electric Power Systems Research, Volume 77, Issue 11, September 2007, pp. 1514-1520.

[10] A. Morched, L. Martí, J. Ottevangers, "A high-frequency transformer model for the EMTP", IEEE Trans. on Power Delivery, Vol. 8-3, pp. 1615-1626, Jul. 1993

[11] P.T.M. Vaessen, "Transformer model for high frequencies", IEEE Transactions on Power Delivery, vol. 3-4, pp. 1761-1768, October 1988.

[12] D.J. Wilcox, W.G. Hurley, T.P. McHale, M. Conlon, "Application of modified modal theory in the modelling of practical transformers", IEE Proceedings-C, Vol. 139-6, pp. 513-520, Nov. 1992.

[13] T. Noda, H. Nakamoto, S. Yokoyama, "Accurate Modeling of Core-Type Distribution Transformers for Electromagnetic Transient Studies",

IEEE Transactions on Power Delivery, Vol. 17, No. 4, pp. 969-976, October 2002.
[14] B. Gustavsen, "Wide Band Modeling of Power Transformers", IEEE Transactions on Power Delivery, Vol. 19, No. 1, pp. 414-422, January 2004.
[15] B. Gustavsen, "Frequency-dependent modeling of power transformers with ungrounded windings", IEEE Transactions on Power Delivery, vol. 19-3, pp. 1328–1334, July 2004.
[16] A. Greenwood, M. Glinkowski, "Voltage Escalation in Vacuum Switching Operations", IEEE Trans. on Power Delivery, vol. 3-4, pp. 1698–1706, Oct. 1988.
[17] M.T. Glinkowski, M.R. Gutierrez, D. Braun, "Voltage Escalation and Reignition Behaviour of Vacuum Generator Circuit Breakers During Load Shedding", IEEE Trans. on Power Delivery, vol. 12-1, pp. 219–226, Jan. 1997.
[18] M. Popov, L. van der Sluis, G. C. Paap, Investigation of the Circuit Breaker Reignition Overvoltages Caused by No-load Transformer Switching Surges, ETEP Vol. 11, No. 6, November/December 2001.
[19] J. Kosmuc, I. Zunko, "A Statistical Vacuum Circuit Breaker Model for Simulation of Transient Overvoltages" IEEE Trans. on Power Delivery, vol. 10-1, pp. 294-300, 1995.
[20] L. Czarnecki, M. Lindmayer, "Measurement and Statistical Simulation of Virtual Current Chopping in Vacuum Switches", Proc. of the 11th International Symposium on Discharges and Electrical Insulation in Vacuum (ISDEIV), Berlin, 1984.
[21] J. Helmer, M. Lindmayer, "Mathematical modeling of the high frequency behavior of vacuum interrupters and comparison with measured transients in power systems", Proc. of the 17th International Symposium on Discharges and Electrical Insulation in Vacuum (ISDEIV), 21-26 July 1996, vol. 1, pp. 323 – 331.
[22] A. H. Moore and T. J. Blalock, "Extensive Field measurements support new approach to Protection of Arc Furnace Transformers against Switching Transients", IEEE Trans. on Power Apparatus and Systems, vol. PAS – 94, no. 2, March/April 1975.
[23] S.M. Wong, L.A. Snider and E.W.C. Lo, "Overvoltages and Reignition behaviour of Vacuum Circuit Breaker", Proc. of the International Conference on Power System Transients – IPST 2003, New Orleans, Louisiana, USA, September 28 - October 2, 2003.
[24] R.P.P. Smeets, T. Funahashi, E. Kaneko, I. Ohshima, "Types of reignition following high-frequency current zero in vacuum interrupters with two types of contact material", IEEE Trans. on Plasma Science, vol. 21-5, Oct. 1993. pp: 478 – 483.
[25] H. Dommel: "EMTP Theory Book", April 1996, Microtran Power System Analysis Corporation.
[26] W. Xu, H. Dommel and J. Marti: "A synchronous machine model for three-phase harmonic analysis and EMTP initialization", IEEE Trans. on Power Systems, Vol. 6, No. 4, November 1991, pp. 1530-1538.
[27] G. J. Rogers, D. Shirmohammadi, "Induction machine modeling for electromagnetic transient program", IEEE Trans. on energy Conversion, Vol EC-2, No. 4, December 1987.
[28] Electromagnetic Transients Program (EMTP), EMTP-V3 Rule Book I, Development Coordination Group of EMTP, 1996.
[29] K.J. Cornick, T.R. Thompson, "Steep fronted switching voltage transients and their distribution in motor windings, Part 1: System measurements of steep-fronted switching voltage transient", Proc. EE, vol. 129. Pt. B. March 1982.
[30] E.P. Dick, B. K. Gupta, P. Pilai, A. Narang, T.S. Lauber, D.K. Sharma, "Prestriking voltages associated with motor breaker closing", IEEE Trans. Energy Conversion, vol. 3, no. 4, Dec. 1988.
[31] J.L. Guardado, V. Venegas, E. Melgoza K. J. Cornick J. L. Naredo, "Transient Overvoltages in Electrical Motors During Sequential Pole Closure", IEEE Trans. on Energy Conversion, Vol. 14-4, Dec. 1999.
[32] M.I. Samesima, J.C. de Oliveira, E.M. Dias, "Frequency response analysis and modeling of measurement transformers under distorted current and voltage supply", IEEE Trans. on Power Delivery, vol.6 , issue: 4, 1991, pp: 1762 – 1768.
[33] B. K. Rao and G. Gajjar, "Development and Application of Vacuum Circuit Breaker Model in Electromagnetic Transient Simulation", 2006 IEEE Power India Conference.